Regional Climatic Model RegCM User Manual
Version 4.3

Nellie Elguindi, Xunqiang Bi, Filippo Giorgi, Badrinath Nagarajan,
Jeremy Pal, Fabien Solmon, Sara Rauscher, Ashraf Zakey and Graziano Giuliani
Trieste, Italy
May 2011

Acknowledgements

Contents

List of Figures

List of Tables

Chapter 1

The RegCM

The RegCM is a regional climate model developed throughout the years, with a wide base of model users. It has evolved from the first version developed in the late eighties (RegCM1, *Dickinson et al.* [1989]), *Giorgi* [1990]), to later versions in the early nineties (RegCM2, *Giorgi et al.* [1993b], *Giorgi et al.* [1993c]), late nineties (RegCM2.5, *Giorgi and Mearns* [1999]) and 2000s (RegCM3, *Pal et al.* [2000]).

The RegCM has been the first limited area model developed for long term regional climate simulation, it has participated to numerous regional model intercomparison projects, and it has been applied by a large community for a wide range of regional climate studies, from process studies to paleo-climate and future climate projections (*Giorgi and Mearns* [1999], *Giorgi et al.* [2006]).

The RegCM system is a community model, and in particular it is designed for use by a varied community composed by scientists in industrialized countries as well as developing nations (*Pal et al.* [2007]).

As such, it is designed to be a public, open source, user friendly and portable code that can be applied to any region of the World. It is supported through the Regional Climate research NETwork, or RegCNET, a widespread network of scientists coordinated by the Earth System Physics section of the Abdus Salam International Centre for Theoretical Physics Abdus Salam International Centre for Theoretical Physics (ICTP), being the foster the growth of advanced studies and research in developing countries one of the main aims of the ICTP.

The home of the model is:

http://users.ictp.it/RegCNET

Scientists across this network (currently subscribed by over 750 participants) can communicate through an email list and via regular scientific workshops, and they have been essential for the evaluation and sequential improvements of the model.

Since the release of RegCM3 described by *Pal et al.* [2007], the model has undergone a substantial evolution both in terms of software code and physics representations, and this has lead to the development of a fourth version of the model, RegCM4, which was released by the ICTP in June 2010 as a prototype version (RegCM4.0) and in May 2011 as a first complete version (RegCM4.1).

The purpose of this Manual is to provide a basic reference for RegCM4, with a description of the model, with a special accent to the improvements recently introduced. Compared to previous versions, RegCM4 includes new land surface, planetary boundary layer and air-sea flux schemes, a mixed convection and tropical band configuration, modifications to the pre-existing radiative transfer and boundary layer schemes and a full upgrade of the model code towards improved flexibility, portability and user friendliness.

The model can be interactively coupled to a 1D lake model, a simplified aerosol scheme (including OC, BC, SO4, dust and sea spray) and a gas phase chemistry module (CBM-Z). Overall, RegCM4 shows an improved performance in several respects compared to previous versions, although further testing by the user community is needed to fully explore its sensitivities and range of applications.

The RegCM is available on the World Wide Web thanks to the Democritos Italy CNR group at:

https://eforge.escience-lab.org/gf/project/regcm

Chapter 2

Description

2.1 History

The idea that limited area models (LAMs) could be used for regional studies was originally proposed by *Dickinson et al.* [1989] and *Giorgi* [1990].

This idea was based on the concept of one-way nesting, in which large scale meteorological fields from General Circulation Model (GCM) runs provide initial and time-dependent meteorological lateral boundary conditions (LBCs) for high resolution Regional Climate Model (RCM) simulations, with no feedback from the RCM to the driving GCM.

The first generation NCAR RegCM was built upon the National Center for Atmospheric Research (NCAR)-Pennsylvania State University (PSU) Mesoscale Model version 4 (MM4) in the late 1980s [*Dickinson et al.*, 1989; *Giorgi*, 1989]. The dynamical component of the model originated from the MM4, which is a compressible, finite difference model with hydrostatic balance and vertical σ-coordinates.

Later, the use of a split-explicit time integration scheme was added along with an algorithm for reducing horizontal diffusion in the presence of steep topographical gradients [*Giorgi et al.*, 1993a, b].

As a result, the dynamical core of the RegCM is similar to that of the hydrostatic version of Mesoscale Model version 5 (MM5) [*Grell et al.*, 1994]: the RegCM4 is thus a hydrostatic, compressible, sigma-p vertical coordinate model run on an Arakawa B-grid in which wind and thermodynamical variables are horizontally staggered using a time-splitting explicit integration scheme in which the two fastest gravity modes are first separated from the model solution and then integrated with smaller time steps.

For application of the MM4 to climate studies, a number of physics parameterizations were replaced, mostly in the areas of radiative transfer and land surface physics, which led to the first generation RegCM [*Dickinson et al.*, 1989; *Giorgi*, 1990]. The first generation RegCM included the Biosphere-Atmosphere Transfer Scheme, BATS, [*Dickinson et al.*, 1986] for surface process representation, the radiative transfer scheme of the Community Climate Model version 1 (CCM1), a medium resolution local planetary boundary layer scheme, the Kuo-type cumulus convection scheme of [*Anthes*, 1977] and the explicit moisture scheme of [*Hsie et al.*, 1984].

A first major upgrade of the model physics and numerical schemes was documented by [*Giorgi et al.*, 1993a, b], and resulted in a second generation RegCM, hereafter referred to as REGional Climate Model version 2 (RegCM2). The physics of RegCM2 was based on that of the NCAR Community Climate Model version 2 (CCM2) [*Hack et al.*, 1993], and the mesoscale model MM5 [*Grell et al.*, 1994]. In particular, the CCM2 radiative transfer package [*Briegleb*, 1992] was used for radiation calculations, the non local boundary layer scheme of [*Holtslag et al.*, 1990] replaced the older local scheme, the mass flux cumulus cloud scheme of [*Grell*, 1993] was added as an option, and the latest version of BATS1E [*Dickinson et al.*, 1993] was included in the model.

In the last few years, some new physics schemes have become available for use in the RegCM, mostly based on physics schemes of the latest version of the Community Climate Model (CCM), Community Climate Model version 3 (CCM3) [*Kiehl et al.*, 1996]. First, the CCM2 radiative transfer package has been replaced by that of the CCM3. In the CCM2 package, the effects of H_2O, O_3, O_2, CO_2 and clouds were accounted for by the model. Solar radiative transfer was treated with a δ-Eddington approach and cloud radiation depended on three cloud parameters, the cloud fractional cover, the cloud liquid water content, and the cloud effective droplet radius. The CCM3 scheme retains the same structure as that of the CCM2, but it includes new features such as the effect of additional greenhouse gases (NO_2, CH_4, CFCs), atmospheric aerosols, and cloud ice. Scattering and absorption of

solar radiation by aerosols are also included based on the aerosol optical properties (Absorption Coefficient and Single Scattering Albedo).

A simplified explicit moisture scheme *Hsie et al.* [1984] is included, where only a prognostic equation for cloud water is used, which accounts for cloud water formation, advection and mixing by turbulence, re-evaporation in sub-saturated conditions, and conversion into rain via a bulk autoconversion term. Prognosed cloud water variable is directly used in the cloud radiation calculations, and not diagnosed in terms of the local relative humidity, adding a very important and far reaching element of interaction between the simulated hydrologic cycle and energy budget calculations.

The solar spectrum optical properties are based on the cloud liquid water path, which is in turn based on the cloud liquid water amount prognostically calculated by the model, cloud fractional cover, which is calculated diagnostically as a function of relative humidity, and effective cloud droplet radius, which is parameterized as a function of temperature and land sea mask for liquid water and as a function of height for ice phase.

In addition, the scheme diagnostically calculates a fraction of cloud ice as a function of temperature. In the infrared spectrum the cloud emissivity is calculated as a function of cloud liquid/ice water path and cloud infrared absorption cross sections depending on effective radii for the liquid and ice phase.

One of the problems in this formulation is that the scheme uses the cloud fractional cover to produce grid box mean cloud properties which are then treated as if the entire grid box was covered by an effectively thinner cloud layer. However, because of the non-linear nature of radiative transfer, this approach tends to produce a grayer mean grid box than if separate cloudy and clear sky fractional fluxes were calculated. By taking advantage of the fact that the scheme also calculates clear sky fluxes for diagnostic purposes, in iRegCM4 we modified this radiative cloud representation by first calculating the total cloud cover at a given grid point and then calculating the surface fluxes separately for the cloudy and clear sky portions of the grid box.

The total cloud cover at a model grid box is given by a value intermediate between that obtained using the random overlap assumption (which maximizes cloud cover) and that given by the largest cloud cover found in any single layer of the column overlying the grid box (which implies a full overlap and it is thus is a minimum estimate of total cloud cover).

This modification thus accounts for the occurrence of fractional clear sky at a given grid box, leading to more realistic grid-box average surface radiative fluxes in fractional cloudy conditions.

A large-scale cloud and precipitation scheme which accounts for the subgrid-scale variability of clouds [*Pal et al.*, 2000], parameterizations for ocean surface fluxes [*Zeng et al.*, 1998], and multiple cumulus convection scheme [*Anthes*, 1977; *Grell*, 1993; *Emanuel*, 1991; *Emanuel and Zivkovic-Rothman*, 1999] are the same as in RegCM3, but a new "mixed scheme" Grell+Emanuel is introduced: it allows the user to select one of the two schemes in function of the ocean-land mask.

The other main development compared to RegCM3 concerns the aerosol radiative transfer calculations. In RegCM3 the aerosol radiative forcing was based on three dimensional fields produced by the aerosol model, and included only scattering and absorption in the shortwave spectrum (see *Giorgi et al.* [2002]). In RegCM4 we added the contribution of the infrared spectrum following *Solmon et al.* [2008].

This is especially important for relatively large dust and sea salt particles and it is calculated by introducing an aerosol infrared emissivity calculated as a function of aerosol path and absorption cross section estimated from aerosol size distribution and long wave refractive indices. Long wave diffusion, which could be relevant for larger dust particles, is not treated as part of this scheme.

The mosaic-type parameterization of subgrid-scale heterogeneity in topography and land use [*Giorgi et al.*, 2003b] allows finer surface resolution in the Biosphere-Atmosphere Transfer Scheme version 1e (BATS1e).

2.2 Model components

The RegCM modeling system has four components: Terrain, ICBC, RegCM, and Postprocessor. Terrain and ICBC are the two components of RegCM preprocessor. Terrestrial variables (including elevation, landuse and sea surface temperature) and three-dimensional isobaric meteorological data are horizontally interpolated from a latitude-longitude mesh to a high-resolution domain on either a Rotated (and Normal) Mercator, Lambert Conformal, or Polar Stereographic projection. Vertical interpolation from pressure levels to the σ coordinate system of RegCM is also performed. σ surfaces near the ground closely follow the terrain, and the higher-level σ surfaces tend to approximate isobaric surfaces.

Since the vertical and horizontal resolution and domain size can vary, the modeling package programs employ
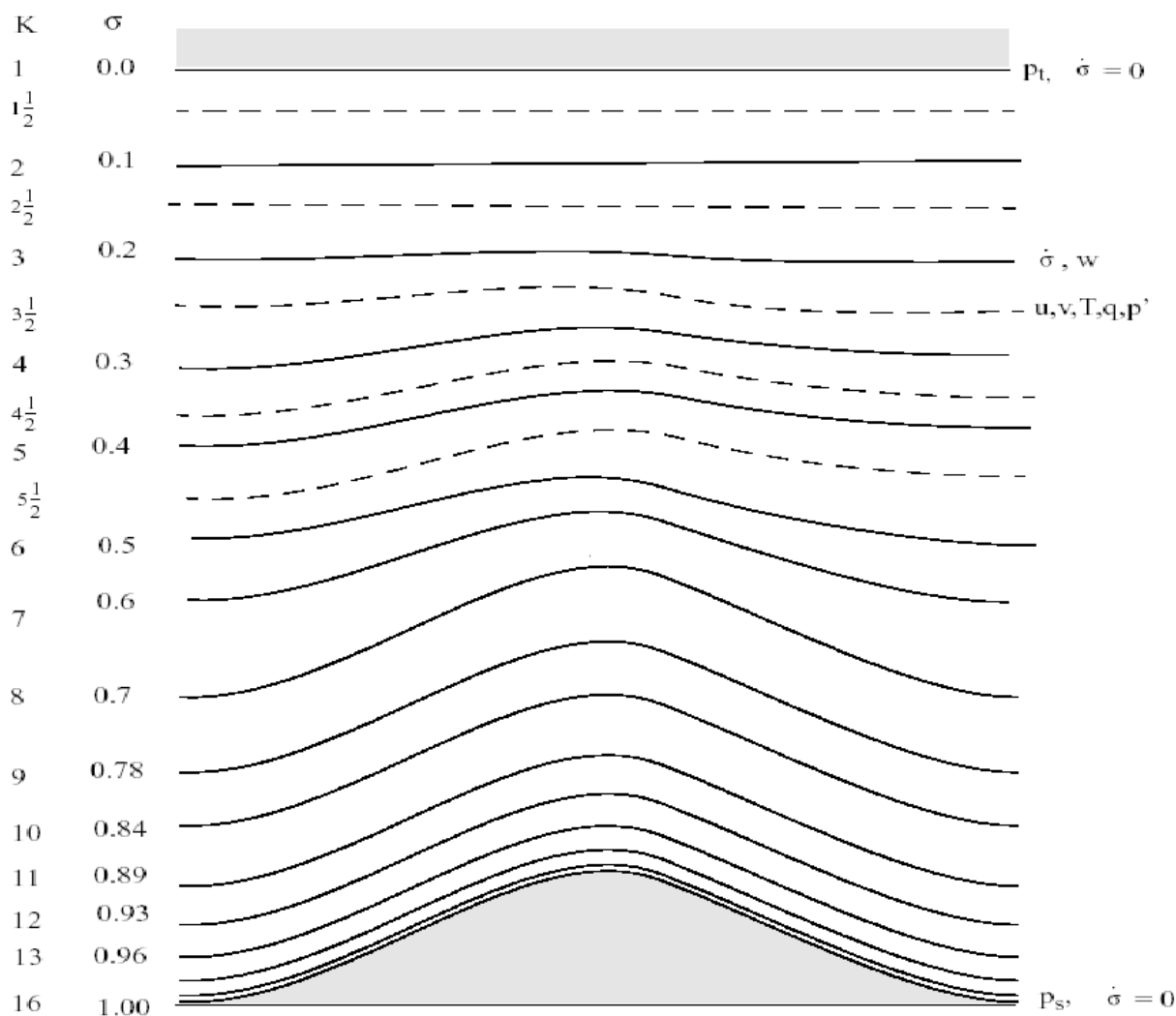
Figure 2.1: Schematic representation of the vertical structure of the model. This example is for 16 vertical layers. Dashed lines denote half-sigma levels, solid lines denote full-sigma levels. (Adapted from the PSU/NCAR Mesoscale Modeling System Tutorial Class Notes and User's Guide.)

parameterized dimensions requiring a variable amount of core memory, and the requisite hard-disk storage amount is varied accordingly.

2.3   The RegCM Model Horizontal and Vertical Grid

It is useful to first introduce the model's grid configuration. The modeling system usually gets and analyzes its data on pressure surfaces, but these have to be interpolated to the model's vertical coordinate before input to the model. The vertical coordinate is terrain-following (Figure 2.1) meaning that the lower grid levels follow the terrain while the upper surface is flatter. Intermediate levels progressively flatten as the pressure decreases toward the top of the model. A dimensionless σ coordinate is used to define the model levels where p is the pressure, p_t is a specified constant top pressure, p_s is the surface pressure.

$$\sigma = \frac{(p - p_t)}{(p_s - p_t)} \tag{2.1}$$

It can be seen from the equation and Figure 2.1 that σ is zero at the top and one at the surface, and each model level is defined by a value of σ. The model vertical resolution is defined by a list of values between zero and one
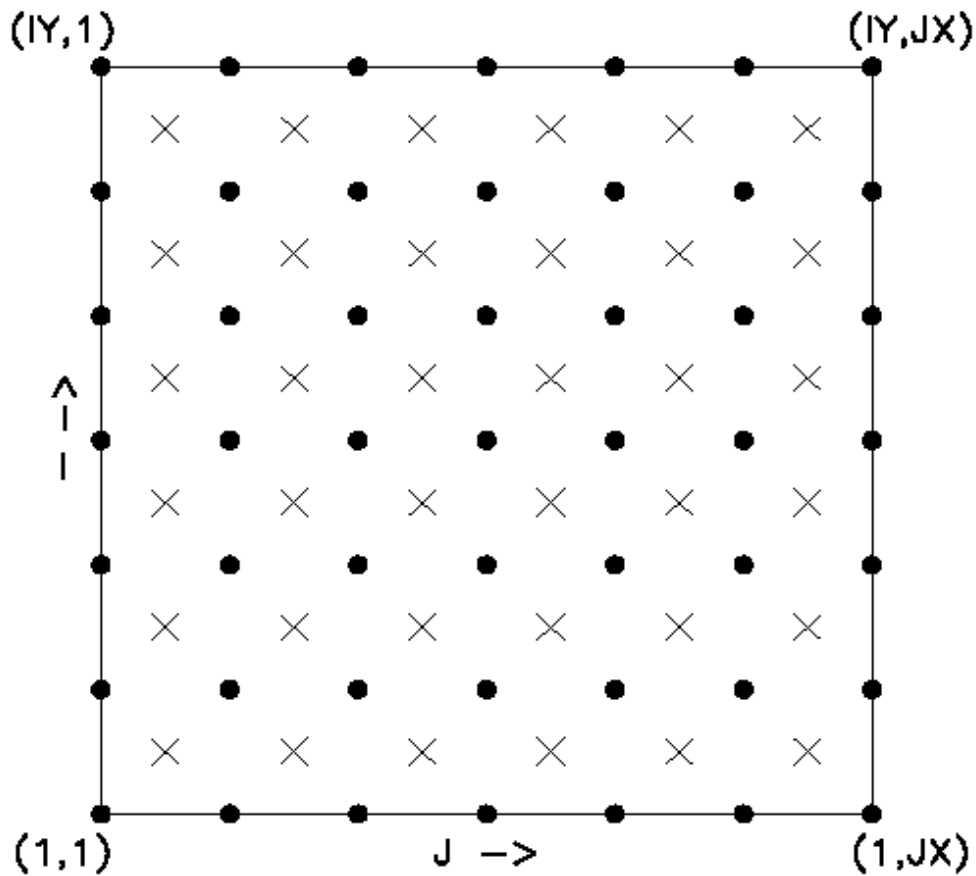
Figure 2.2: Schematic representation showing the horizontal Arakawa B-grid staggering of the dot and cross grid points.

that do not necessarily have to be evenly spaced. Commonly the resolution in the boundary layer is much finer than above, and the number of levels may vary upon the user demand.

The horizontal grid has an Arakawa-Lamb B-staggering of the velocity variables with respect to the scalar variables. This is shown in Figure 2.2 where it can be seen that the scalars (T, q, p, etc) are defined at the center of the grid box, while the eastward (u) and northward (v) velocity components are collocated at the corners. The center points of grid squares will be referred to as cross points, and the corner points are dot points. Hence horizontal velocity is defined at dot points. Data is input to the model, the preprocessors do the necessary interpolation to assure consistency with the grid.

All the above variables are defined in the middle of each model vertical layer, referred to as half-levels and represented by the dashed lines in Figure 2.1. Vertical velocity is carried at the full levels (solid lines). In defining the sigma levels it is the full levels that are listed, including levels at $\sigma = 0$ and 1. The number of model layers is therefore always one less than the number of full sigma levels.

The finite differencing in the model is, of course, crucially dependent upon the grid staggering wherever gradients or averaging are represented terms in the equation.

2.4 Map Projections and Map-Scale Factors

The modeling system has a choice of four map projections. Lambert Conformal is suitable for mid-latitudes, Polar Stereographic for high latitudes, Normal Mercator for low latitudes, and Rotated Mercator for extra choice. The

x and *y* directions in the model do not correspond to west-east and north-south except for the Normal Mercator projection, and therefore the observed wind generally has to be rotated to the model grid, and the model *u* and *v* components need to be rotated before comparison with observations. These transformations are accounted for in the model pre-processors that provide data on the model grid (Please note that model output of u and v components, raw or postprocessed, should be rotated to a lat/lon grid before comparing to observations). The map scale factor, *m*, is defined by

$$m = \text{(distance on grid) / (actual distance on earth)}$$

and its value is usually close to one, varying with latitude. The projections in the model preserve the shape of small areas, so that dx=dy everywhere, but the grid length varies across the domain to allow a representation of a spherical surface on a plane surface. Map-scale factors need to be accounted for in the model equations wherever horizontal gradients are used.

Chapter 3

Model Physics

3.1 Dynamics

The model dynamic equations and numerical discretization are described by *Grell et al.* [1994].

3.1.1 Horizontal Momentum Equations

$$\frac{\partial p^* u}{\partial t} = -m^2 \left(\frac{\partial p^* uu/m}{\partial x} + \frac{\partial p^* vu/m}{\partial y} \right) - \frac{\partial p^* u \dot{\sigma}}{\partial \sigma}$$

$$-mp^* \left[\frac{RT_v}{(p^* + p_t/\sigma)} \frac{\partial p^*}{\partial x} + \frac{\partial \phi}{\partial x} \right] + f p^* v + F_H u + F_V u, \tag{3.1}$$

$$\frac{\partial p^* v}{\partial t} = -m^2 \left(\frac{\partial p^* uv/m}{\partial x} + \frac{\partial p^* vv/m}{\partial y} \right) - \frac{\partial p^* v \dot{\sigma}}{\partial \sigma}$$

$$-mp^* \left[\frac{RT_v}{(p^* + p_t/\sigma)} \frac{\partial p^*}{\partial y} + \frac{\partial \phi}{\partial y} \right] + f p^* u + F_H v + F_V v, \tag{3.2}$$

where u and v are the eastward and northward components of velocity, T_v is virtual temperature, ϕ is geopotential height, f is the coriolis parameter, R is the gas constant for dry air, m is the map scale factor for either the Polar Stereographic, Lambert Conformal, or Mercator map projections, $\dot{\sigma} = \frac{d\sigma}{dt}$, and F_H and F_V represent the effects of horizontal and vertical diffusion, and $p^* = p_s - p_t$.

3.1.2 Continuity and Sigmadot ($\dot{\sigma}$) Equations

$$\frac{\partial p^*}{\partial t} = -m^2 \left(\frac{\partial p^* u/m}{\partial x} + \frac{\partial p^* v/m}{\partial y} \right) - \frac{\partial p^* \dot{\sigma}}{\partial \sigma}. \tag{3.3}$$

The vertical integral of Equation 3.3 is used to compute the temporal variation of the surface pressure in the model,

$$\frac{\partial p^*}{\partial t} = -m^2 \int_0^1 \left(\frac{\partial p^* u/m}{\partial x} + \frac{\partial p^* v/m}{\partial y} \right) d\sigma. \tag{3.4}$$

After calculation of the surface-pressure tendency $\frac{\partial p^*}{\partial t}$, the vertical velocity in sigma coordinates ($\dot{\sigma}$) is computed at each level in the model from the vertical integral of Equation 3.3.

$$\dot{\sigma} = -\frac{1}{p^*} \int_0^\sigma \left[\frac{\partial p^*}{\partial t} + m^2 \left(\frac{\partial p^* u/m}{\partial x} + \frac{\partial p^* v/m}{\partial y} \right) \right] d\sigma\prime \tag{3.5}$$

where $\sigma\prime$ is a dummy variable of integration and $\dot{\sigma}(\sigma = 0) = 0$.

3.1.3   Thermodynamic Equation and Equation for Omega (ω)

The thermodynamic equation is

$$\frac{\partial p^* T}{\partial t} = -m^2 \left(\frac{\partial p^* uT/m}{\partial x} + \frac{\partial p^* vT/m}{\partial y} \right) - \frac{\partial p^* T \dot{\sigma}}{\partial \sigma} +$$

$$\frac{RT_v \omega}{c_{pm}(\sigma + P_t/p_{ast})} + \frac{p^* Q}{c_{pm}} + F_H T + F_V T \tag{3.6}$$

where c_{pm} is the specific heat for moist air at constant pressure, Q is the diabatic heating, $F_H T$ represents the effect of horizontal diffusion, $F_V T$ represents the effect of vertical mixing and dry convective adjustment, and ω is

$$\omega = p^* \dot{\sigma} + \sigma \frac{dp^*}{dt} \tag{3.7}$$

where,

$$\frac{dp^*}{dt} = \frac{\partial p^*}{\partial t} + m \left(u \frac{\partial p^*}{\partial x} + v \frac{\partial p^*}{\partial y} \right) \tag{3.8}$$

The expression for $c_{pm} = c_p(1 + 0.8q_v)$, where c_p is the specific heat at constant pressure for dry air and q_v is the mixing ratio of water vapor.

3.1.4   Hydrostatic Equation

The hydrostatic equation is used to compute the geopotential heights from the virtual temperature T_v,

$$\frac{\partial \phi}{\partial ln(\sigma + p_t/p^*)} = -RT_v \left[1 + \frac{q_c + q_r}{1 + q_v} \right]^{-1} \tag{3.9}$$

where $T_v = T(1 + 0.608q_v)$, q_v, q_c, and q_r are the water vapor, cloud water or ice, and rain water or snow, mixing ratios.

3.2 Physics parametrizations

3.2.1 Radiation Scheme

RegCM4 uses the radiation scheme of the NCAR CCM3, which is described in *Kiehl et al.* [1996]. Briefly, the solar component, which accounts for the effect of O_3, H_2O, CO_2, and O_2, follows the δ-Eddington approximation of *Kiehl et al.* [1996]. It includes 18 spectral intervals from 0.2 to 5 μm. The cloud scattering and absorption parameterization follow that of *Slingo* [1989], whereby the optical properties of the cloud droplets (extinction optical depth, single scattering albedo, and asymmetry parameter) are expressed in terms of the cloud liquid water content and an effective droplet radius. When cumulus clouds are formed, the gridpoint fractional cloud cover is such that the total cover for the column extending from the model-computed cloud-base level to the cloud-top level (calculated assuming random overlap) is a function of horizontal gridpoint spacing. The thickness of the cloud layer is assumed to be equal to that of the model layer, and a different cloud water content is specified for middle and low clouds.

3.2.2 Land Surface Models

BATS (default): BATS is a surface package designed to describe the role of vegetation and interactive soil moisture in modifying the surface-atmosphere exchanges of momentum, energy, and water vapor (see *Dickinson et al.* [1993] for details). The model has a vegetation layer, a snow layer, a surface soil layer, 10 cm thick, or root zone layer, 1-2 m thick, and a third deep soil layer 3 m thick. Prognostic equations are solved for the soil layer temperatures using a generalization of the force-restore method of *Deardoff* [1978]. The temperature of the canopy and canopy foilage is calculated diagnostically via an energy balance formulation including sensible, radiative, and latent heat fluxes.

The soil hydrology calculations include predictive equations for the water content of the soil layers. These equations account for precipitation, snowmelt, canopy foilage drip, evapotranspiration, surface runoff, infiltration below the root zone, and diffusive exchange of water between soil layers. The soil water movement formulation is obtained from a fit to results from a high-resolution soil model *Dickinson* [1984] and the surface runoff rates are expressed as functions of the precipitation rates and the degree of soil water saturation. Snow depth is prognostically calculated from snowfall, snowmelt, and sublimation. Precipitation is assumed to fall in the form of snow if the temperature of the lowest model level is below 271 K.

Sensible heat, water vapor, and momentum fluxes at the surface are calculated using a standard surface drag coefficient formulation based on surface-layer similarity theory. The drag coefficient depends on the surface roughness length and on the atmospheric stability in the surface layer. The surface evapotranspiration rates depend on the availability of soil water. Biosphere-Atmosphere Transfer Scheme (BATS) has 20 vegetation types (Table 3.2; soil textures ranging from coarse (sand), to intermediate (loam), to fine (clay); and different soil colors (light to dark) for the soil albedo calculations. These are described in *Dickinson et al.* [1986].

In the latest release version, additional modifications have been made to BATSin order to account for the subgrid variability of topography and landcover using a mosaic-type approach [*Giorgi et al.*, 2003a]. Thismodification adopts a regular fine-scale surface subgrid for eachcoarse model grid cell. Meteorological variables are disaggregatedfrom the coarse grid to the fine grid based on the elevationdifferences. The BATS calculations are then performed separatelyfor each subgrid cell, and surface fluxes are reaggregated onto thecoarse grid cell for input to the atmospheric model. This parameterization showed a marked improvement in the representation ofthe surface hydrological cycle in mountainous regions [*Giorgi et al.*, 2003a]. As a first augmentation, in REGional Climate Model version 4 (RegCM4) two new land use types were added to BATS to represent urban and sub-urban environments. Urban development not only modifies the surface albedo and alters the surface energy balance, but also creates impervious surfaces with large effects on runoff and evapotranspiration. These effects can be described by modifying relevant properties of the land surface types in the BATS package, such as maximum vegetation cover, roughness length, albedo, and soil characteristics. For this purpose, we implemented the parameters proposed in Table 1 of *Kueppers et al.* [2008].

CLM (optional): The Community Land Model (CLM; *Oleson et al.* [2008]) is the land surface model developed by the National Center of Atmospheric Research (NCAR) as part of the Community Climate System Model (CCSM), described in detail in *Collins et al.* [2006]. CLM version 3.5 was coupled to RegCM for a more detailed land surface description option. CLM contains five possible snow layers with an additional representation of trace snow and ten unevenly spaced soil layers with explicit solutions of temperature, liquid water and ice water in each layer. To account for land surface complexity within a climate model grid cell, CLM uses a tile or mosaic approach

Table 3.1: Land Cover/Vegetation classes

1.	Crop/mixed farming
2.	Short grass
3.	Evergreen needleleaf tree
4.	Deciduous needleleaf tree
5.	Deciduous broadleaf tree
6.	Evergreen broadleaf tree
7.	Tall grass
8.	Desert
9.	Tundra
10.	Irrigated Crop
11.	Semi-desert
12.	Ice cap/glacier
13.	Bog or marsh
14.	Inland water
15.	Ocean
16.	Evergreen shrub
17.	Deciduous shrub
18.	Mixed Woodland
19.	Forest/Field mosaic
20.	Water and Land mixture

to capture surface heterogeneity. Each CLM gridcell contains up to four different land cover types (glacier, wetland, lake, and vegetated), where the vegetated fraction can be further divided into 17 different plant functional types. Hydrological and energy balance equations are solved for each land cover type and aggregated back to the gridcell level. A detailed discussion of CLM version 3 implemented in RegCM3 and comparative analysis of land surface parameterization options is presented in *Steiner et al.* [2009]. Since CLM was developed for the global scale, several input files and processes were modified to make it more appropriate for regional simulations, including (1) the use of high resolution input data, (2) soil moisture initialization, and (3) and an improved treatment of grid cells along coastlines. For the model input data, CLM requires several time-invariant surface input parameters: soil color, soil texture, percent cover of each land surface type, leaf and stem area indices, maximum saturation fraction, and land fraction [*Lawrence and Chase*, 2007]. Table 3.3 shows the resolution for each input parameter used at the regional scale in RegCM-CLM compared to resolutions typically used for global simulations. The resolution of surface input parameters was increased for several parameters to capture surface heterogeneity when interpolating to the regional climate grid. Similar to *Lawrence and Chase* [2007], the number of soil colors was extended from 8 to 20 classes to resolve regional variations. The second modification was to update the soil moisture initialization based on a climatological soil moisture average [*Giorgi and Bates*, 1989] over the use of constant soil moisture content throughout the grid generally used for global CLM. By using a climatological average for soil moisture, model spin-up time is reduced with regards to deeper soil layers. The third modification to the CLM is the inclusion of a mosaic approach for gridcells that contain both land and ocean surface types. With this approach, a weighted average of necessary surface variables was calculated for land/ocean gridcells using the land fraction input dataset. This method provides a better representation of coastlines using the high-resolution land fraction data described in Table 3.3. For a more detailed description of CLM physics parameterizations see *Oleson* [2004].

Table 3.2: BATS vegetation/land-cover

Parameter	Land Cover/Vegetation Type																			
	1	2	3	4	5	6	7	8	9	10	11	12	13	14	15	16	17	18	19	20
Max fractional vegetation cover	0.85	0.80	0.80	0.80	0.80	0.90	0.80	0.00	0.60	0.80	0.35	0.00	0.80	0.00	0.00	0.80	0.80	0.80	0.80	0.80
Difference between max fractional vegetation cover and cover at 269 K	0.6	0.1	0.1	0.3	0.5	0.3	0.0	0.2	0.6	0.1	0.0	0.4	0.0	0.0	0.2	0.3	0.2	0.4	0.4	
Roughness length (m)	0.08	0.05	1.00	1.00	0.80	2.00	0.10	0.05	0.04	0.06	0.10	0.01	0.03	0.0004	0.0004	0.10	0.10	0.80	0.3	0.3
Displacement height (m)	0.0	0.0	9.0	9.0	0.0	18.0	0.0	0.0	0.0	0.0	0.0	0.0	0.0	0.0	0.0	0.0	0.0	0.0	0.0	0.0
Min stomatal resistence (s/m)	45	60	80	80	120	60	60	200	80	45	150	200	45	200	200	80	120	100	120	120
Max Leaf Area Index	6	2	6	6	6	6	6	0	6	6	6	0	6	0	0	6	6	6	6	6
Min Leaf Area Index	0.5	0.5	5	1	1	5	0.5	0	0.5	0.5	0.5	0	0.5	0	0	5	1	3	0.5	0.5
Stem (dead matter area index)	0.5	4.0	2.0	2.0	2.0	2.0	2.0	0.5	0.5	2.0	2.0	2.0	2.0	2.0	2.0	2.0	2.0	2.0	2.0	2.0
Inverse square root of leaf dimension ($m^{-1/2}$)	10	5	5	5	5	5	5	5	5	5	5	5	5	5	5	5	5	5	5	5
Light sensitivity factor ($m^2 W^{-1}$)	0.02	0.02	0.06	0.06	0.06	0.06	0.02	0.02	0.02	0.02	0.02	0.02	0.02	0.02	0.02	0.02	0.02	0.06	0.02	0.02
Upper soil layer depth (mm)	100	100	100	100	100	100	100	100	100	100	100	100	100	100	100	100	100	100	100	100
Root zone soil layer depth (mm)	1000	1000	1500	1500	2000	1500	1000	1000	1000	1000	1000	1000	1000	1000	1000	1000	1000	2000	2000	2000
Depth of total soil (mm)	3000	3000	3000	3000	3000	3000	3000	3000	3000	3000	3000	3000	3000	3000	3000	3000	3000	3000	3000	3000
Soil texture type	6	6	6	6	7	8	6	3	6	6	5	12	6	6	6	6	5	6	6	0
Soil color type	5	3	4	4	4	4	4	1	3	3	2	1	5	5	5	4	3	4	4	0
Vegetation albedo for wavelengths $< 0.7\,\mu$ m	0.10	0.10	0.05	0.05	0.08	0.04	0.08	0.20	0.10	0.08	0.17	0.80	0.06	0.07	0.07	0.05	0.08	0.06	0.06	0.06
Vegetation albedo for wavelengths $> 0.7\,\mu$ m	0.30	0.30	0.23	0.23	0.28	0.20	0.30	0.40	0.30	0.28	0.34	0.60	0.18	0.20	0.20	0.23	0.28	0.24	0.18	0.18

Table 3.3: Resolution for CLM input parameters

Input data	Grid Spacing	Lon range	Lat range
Glacier	0.05° x 0.05°	±179.975	±89.975
Lake	0.05° x 0.05°	±179.975	±89.975
Wetland	0.05° x 0.05°	±179.975	±89.975
Land fraction	0.05° x 0.05°	±179.975	±89.975
LAI/SAI	0.5° x 0.5°	±179.75	±89.75
PFT	0.5° x 0.5°	±179.75	±89.75
Soil color	0.05° x 0.05°	±179.975	±89.975
Soil texture	0.05° x 0.05°	±179.975	±89.975
Max. sat. area	0.5° x 0.5°	±179.75	±89.75

3.2.3 Planetary Boundary Layer Scheme

The planetary boundary layer scheme, developed by *Holtslag et al.* [1990], is based on a nonlocal diffusion concept that takes into account countergradient fluxes resulting from large-scale eddies in an unstable, well-mixed atmosphere. The vertical eddy flux within the PBL is given by

$$F_c = -K_c \left(\frac{\partial C}{\partial z} - \gamma_c \right) \tag{3.10}$$

where γ_c is a "countergradient" transport term describing nonlocal transport due to dry deep convection. The eddy diffusivity is given by the nonlocal formulation

$$K_c = k w_t z \left(1 - \frac{z^2}{h} \right) \tag{3.11}$$

where k is the von Karman constant; w_t is a turbulent convective velocity that depends on the friction velocity, height, and the Monin–Obhukov length; and h is the PBL height.

The countergradient term for temperature and water vapor is given by

$$\gamma_c = C \frac{\phi_c{}^0}{w_t h} \tag{3.12}$$

where C is a constant equal to 8.5, and $\phi_c{}^0$ is the surface temperature or water vapor flux. Equation 3.12 is applied between the top of the PBL and the top of the surface layer, which is assumed to be equal to $0.1h$. Outside this region and for momentum, γ_c is assumed to be equal to 0.

For the calculation of the eddy diffusivity and countergradient terms, the PBL height is diagnostically computed from

$$h = \frac{\text{Ri}_c r [u(h)^2 + v(h)^2]}{(g/\theta_s)[\theta_v(h) - \theta_s]} \tag{3.13}$$

where $u(h)$, $v(h)$, and θ_v are the wind components and the virtual potential temperature at the PBL height, g is gravity, $\text{Ri}_c r$ is the critical bulk Richardson number, and θ_s is an appropriate temperature of are near the surface. Refer to *Holtslag et al.* [1990] and *Holtslag and Boville* [1993] for a more detailed description.

Compared to other schemes this formulation tends to produce relatively strong, and often excessive, turbulent vertical transfer. For example, after extensive testing, we found excessive vertical transfer of moisture in the model resulting in low moisture amounts near the surface and excessive moisture near the PBL top.

Therefore in order to ameliorate this problem, the countergradient term for water vapor was removed in RegCM4. Another problem of the Holtslag scheme (at least in our implementation) is an excessive vertical

transport of heat, moisture and momentum in very stable conditions, such as during the winter in northern hemisphere high latitude regions. For example we found that in such conditions the scheme fails to simulate near surface temperature inversions.

This in turn leads to large warm winter biases (even ¿ 10 degrees) over regions such as Northern Siberia and Northern Canada. As an ad-hoc fix to address this problem, in RegCM4 we implemented the following modification to the scheme:

- We first define very stable conditions within the Holtslag parameterization as conditions in which the ratio of the height from the surface over the Monin-Obhukov length is lower than 0.1.

- When such conditions are found, we set to 0 the eddy diffusivity and counter-gradient terms for all variables.

Preliminary tests showed that this modification reduces the warm bias in high latitude winter conditions and allows the model to better capture surface inversions. These modifications have thus been incorporated as default in the RegCM4 code.

3.2.4 Convective Precipitation Schemes

Convective precipitation is computed using one of three schemes: (1) Modified-Kuo scheme *Anthes* [1977]; (2) Grell scheme *Grell* [1993]; and (3) MIT-Emanuel scheme [*Emanuel*, 1991; *Emanuel and Zivkovic-Rothman*, 1999]. In addition, the Grell parameterization is implemented using one of two closure assumptions: (1) the Arakawa and Schubert closure *Grell et al.* [1994] and (2) the Fritsch and Chappell closure *Fritsch and Chappell* [1980], hereafter refered to as AS74 and FC80, respectively.

1. **Kuo Scheme:** Convective activity in the Kuo scheme is initiated when the moisture convergence M in a column exceeds a given threshold and the vertical sounding is convectively unstable. A fraction of the moisture convergence β moistens the column and the rest is converted into rainfall P^{CU} according to the following relation:

$$P^{CU} \quad = \quad M(1-\beta). \tag{3.14}$$

β is a function of the average relative humidity $\overline{RH}$ of the sounding as follows:

$$\beta \quad = \quad \left\{ \begin{array}{ll} 2(1-\overline{RH}) & \overline{RH} \geq 0.5 \\ 1.0 & \text{otherwise} \end{array} \right\} \tag{3.15}$$

Note that the moisture convergence term includes only the advective tendencies for water vapor. However, evapotranspiration from the previous time step is indirectly included in M since it tends to moisten the lower atmosphere. Hence, as the evapotranspiration increases, more and more of it is converted into rainfall assuming the column is unstable. The latent heating resulting from condensation is distributed between the cloud top and bottom by a function that allocates the maximum heating to the upper portion of the cloud layer. To eliminate numerical point storms, a horizontal diffusion term and a time release constant are included so that the redistributions of moisture and the latent heat release are not performed instantaneously [*Giorgi and Bates*, 1989; *Giorgi and Marinucci*, 1991].

2. **Grell Scheme:** The Grell scheme *Grell* [1993], similar to the AS74 parameterization, considers clouds as two steady-state circulations: an updraft and a downdraft. No direct mixing occurs between the cloudy air and the environmental air except at the top and bottom of the circulations. The mass flux is constant with height and no entrainment or detrainment occurs along the cloud edges. The originating levels of the updraft and downdraft are given by the levels of maximum and minimum moist static energy, respectively. The Grell scheme is activated when a lifted parcel attains moist convection. Condensation in the updraft is calculated by lifting a saturated parcel. The downdraft mass flux (m_0) depends on the updraft mass flux (m_b) according to the following relation:

$$m_0 = \frac{\beta I_1}{I_2} m_b \qquad (3.16)$$

where I_1 is the normalized updraft condensation, I_2 is the normalized downdraft evaporation, and β is the fraction of updraft condensation that re-evaporates in the downdraft. β depends on the wind shear and typically varies between 0.3 and 0.5. Rainfall is given by

$$P^{CU} = I_1 m_b (1 - \beta) \qquad (3.17)$$

Heating and moistening in the Grell scheme are determined both by the mass fluxes and the detrainment at the cloud top and bottom. In addition, the cooling effect of moist downdrafts is included.

Due to the simplistic nature of the Grell scheme, several closure assumptions can be adopted. RegCM4's earlier version directly implements the quasi-equilibrium assumption of AS74. It assumes that convective clouds stabilize the environment as fast as non-convective processes destabilize it as follows:

$$m_b = \frac{ABE'' - ABE}{NA\Delta t} \qquad (3.18)$$

where ABE is the buoyant energy available for convection, ABE'' is the amount of buoyant energy available for convection in addition to the buoyant energy generated by some of the non-convective processes during the time interval Δt, and NA is the rate of change of ABE per unit m_b. The difference $ABE'' - ABE$ can be thought of as the rate of destabilization over time Δt. ABE'' is computed from the current fields plus the future tendencies resulting from the advection of heat and moisture and the dry adiabatic adjustment.

In the latest RegCM4 version, by default, we use a stability based closure assumption, the FC80 type closure assumption, that is commonly implemented in GCMs and RCMs. In this closure, it is assumed that convection removes the ABE over a given time scale as follows:

$$m_b = \frac{ABE}{NA\tau} \qquad (3.19)$$

where τ is the ABE removal time scale.

The fundamental difference between the two assumptions is that the AS74 closure assumption relates the convective fluxes and rainfall to the tendencies in the state of the atmosphere, while the FC80 closure assumption relates the convective fluxes to the degree of instability in the atmosphere. Both schemes achieve a statistical equilibrium between convection and the large-scale processes.

A number of parameters present in the scheme can be used to optimize its performance, and *Giorgi et al.* [1993c] discusses a wide range of sensitivity experiments. We found that the parameter to which the scheme is most sensitive is by and large the fraction of precipitation evaporated in the downdraft (Peff, with values from 0 to 1), which essentially measures the precipitation efficiency. Larger values of Peff lead to reduced precipitation.

3. **MIT-Emanuel scheme:** More detailed descriptions can be found in *Emanuel* [1991] and *Emanuel and Zivkovic-Rothman* [1999]. The scheme assumes that the mixing in clouds is highly episodic and inhomogeneous (as opposed to a continuous entraining plume) and considers convective fluxes based on an idealized model of sub-cloud-scale updrafts and downdrafts. Convection is triggered when the level of neutral buoyancy is greater than the cloud base level. Between these two levels, air is lifted and a fraction of the condensed moisture forms precipitation while the remaining fraction forms the cloud. The cloud is assumed to mix with the air from the environment according to a uniform spectrum of mixtures that ascend or descend to their respective levels of neutral buoyancy. The mixing entrainment and detrainment rates are functions of the vertical gradients of buoyancy in clouds. The fraction of the total cloud base mass flux that

mixes with its environment at each level is proportional to the undiluted buoyancy rate of change with altitude. The cloud base upward mass flux is relaxed towards the sub-cloud layer quasi equilibrium.

In addition to a more physical representation of convection, the MIT-Emanuel scheme offers several advantages compared to the other RegCM4 convection options. For instance, it includes a formulation of the auto-conversion of cloud water into precipitation inside cumulus clouds, and ice processes are accounted for by allowing the auto-conversion threshold water content to be temperature dependent. Additionally, the precipitation is added to a single, hydrostatic, unsaturated downdraft that transports heat and water. Lastly, the MIT-Emanuel scheme considers the transport of passive tracers.

The MIT scheme is the most complex of the three and also includes a number of parameters that can be used to optimize the model performance in different climate regimes. Differently from the Grell scheme, however, test experiments did not identify a single parameter to which the model is most sensitive.

A major augmentation in RegCM4 compared to previous versions of the model is the capability of running different convection schemes over land and ocean, a configuration which we refer to as mixed convection. Extensive test experiments showed that different schemes have different performance over different regions, and in particular over land vs. ocean areas.

For example, the MIT scheme tends to produce excessive precipitation over land areas, especially through the occurrence of very intense individual precipitation events.

In other words, once the scheme is activated, it becomes difficult to decelerate. Conversely, we found that the Grell scheme tends to produce excessively weak precipitation over tropical oceans.

These preliminary tests suggested that a mixed convection approach by which, for example, the MIT scheme is used over oceans and the Grell scheme over land, might be the most suitable option to pursue, and therefore this option was added to the model.

3.2.5 Large-Scale Precipitation Scheme

Subgrid Explicit Moisture Scheme (SUBEX) is used to handle nonconvective clouds and precipitation resolved by the model. This is one of the new components of the model. SUBEX accounts for the subgrid variability in clouds by linking the average grid cell relative humidity to the cloud fraction and cloud water following the work of *Sundqvist et al.* [1989].

The fraction of the grid cell covered by clouds, FC, is determined by,

$$FC = \sqrt{\frac{RH - RH_{min}}{RH_{max} - RH_{min}}} \tag{3.20}$$

where RH_{min} is the relative humidity threshold at which clouds begin to form, and RH_{max} is the relative humidity where FC reaches unity. FC is assumed to be zero when RH is less than RH_{min} and unity when RH is greater than RH_{max}.

Precipitation P forms when the cloud water content exceeds the autoconversion threshold Q^{th}_c according to the following relation:

$$P = C_{ppt}(Q_c/FC - Q_c^{th})FC \tag{3.21}$$

where $1/C_{ppt}$ can be considered the characteristic time for which cloud droplets are converted to raindrops. The threshold is obtained by scaling the median cloud liquid water content equation according to the following:

$$Q^{th}_c = C_{acs}10^{-0.49+0.013T} \tag{3.22}$$

where T is temperature in degrees Celsius, and C_{acs} is the autoconversion scale factor. Precipitation is assumed to fall instantaneously.

SUBEX also includes simple formulations for raindrop accretion and evaporation. The formulation for the accretion of cloud droplets by falling rain droplets is based on the work of *Beheng* [1994] and is as follows:

$$P_{acc} = C_{acc}QP_{sum} \tag{3.23}$$

where P_{acc} is the amount of accreted cloud water, C_{acc} is the accretion rate coefficient, and P_{sum} is the accumulated precipitation from above falling through the cloud.

Precipitation evaporation is based on the work of *Sundqvist et al.* [1989] and is as follows

$$P_{evap} = C_{evap}(1 - RH)P^{1/2}{}_{sum} \tag{3.24}$$

where P_{evap} is the amount of evaporated precipitation, and C_{evap} is the rate coefficient. For a more detailed description of SUBEX and a list of the parameter values refer to *Pal et al.* [2000].

Traditionally, REGional Climate Model version 3 (RegCM3) has shown a tendency to produce excessive precipitation, especially at high resolutions, and optimizations of the in-cloud liquid water threshold for the activation of the autoconversion term *Qcth* and the rate of sub-cloud evaporation *Cevap* parameters have proven effective in ameliorating this problem: greater values of *Qth* and *Cevap* lead to decreased precipitation amounts.

3.2.6 Ocean flux Parameterization

BATS uses standard Monin-Obukhov similarity relations to compute the fluxes with no special treatment of convective and very stable conditions. In addition, the roughness length is set to a constant, i.e. it is not a function of wind and stability.

The Zeng scheme describes all stability conditions and includes a gustiness velocity to account for the additional flux induced by boundary layer scale variability. Sensible heat (SH), latent heat (LH), and momentum (τ) fluxes between the sea surface and lower atmosphere are calculated using the following bulk aerodynamic algorithms,

$$\tau = \rho_a u_*{}^2 (u_x{}^2 + u_y{}^2)^{1/2}/u \tag{3.25}$$

$$\text{SH} = -\rho_a C_{pa} u_* \theta_* \tag{3.26}$$

$$\text{LH} = -\rho_a L_e u_* q_* \tag{3.27}$$

where u_x and u_y are mean wind components, u_* is the frictional wind velocity, θ_* is the temperature scaling parameter, q_* is the specific humidity scaling parameter, ρ_a is air density, C_{pa} is specific heat of air, and L_e is the latent heat of vaporization. For further details on the calculation of these parameters refer to *Zeng et al.* [1998].

3.2.7 Prognostic Sea Surface Skin Temperature Scheme

By default in RegCM, sea surface temperatures (SST) are prescribed every six hours from temporally interpolated weekly or monthly SST products. These products, which are produced from satellite retrievals and in situ measurements, are representative of the mean temperature in the top few meters of the ocean. However, the actual SST can differ significantly from this mean temperature due to the cool-skin and warm-layer effects described by *Fairall et al.* [1996]. To improve the calculation of diurnal fluxes over the ocean, the prognostic SST scheme described by *Zeng* [2005] was implemented in RegCM4. The scheme is based on a two-layer one-dimensional heat transfer model, with the top layer representing the upper few millimeters of the ocean which is cooled by net longwave radiation loss and surface fluxes. The bottom layer is three meters thick, it is warmer by solar radiation and exchanges heat with the top layer. This diurnal SST scheme appears to provide significant, although not major, effects on the model climatology mostly over tropical oceans, for example the Indian ocean, and it is now used as default in RegCM4.

3.2.8 Pressure Gradient Scheme

Two options are available for calculating the pressure gradient force. The normal way uses the full fields. The other way is the hydrostatic deduction scheme which makes use of a perturbation temperature. In this scheme, extra smoothing on the top is done in order to reduce errors related to the PGF calculation.

3.2.9 Lake Model

The lake model developed by *Hostetler et al.* [1993] can be interactively coupled to the atmospheric model. In the lake model, fluxes of heat, moisture, and momentum are calculated based on meteorological inputs and the lake surface temperature and albedo. Heat is transferred vertically between lake model layers by eddy and convective mixing. Ice and snow may cover part or all of the lake surface.

In the lake model, the prognostic equation for temperature is

$$\frac{\partial T}{\partial t} = (k_e + k_m)\frac{\partial^2 T}{\partial z^2} \tag{3.28}$$

where T is the temperature of the lake layer, and k_e and k_m are the eddy and molecular diffusivities, respectively. The parameterization of *Henderson-Sellers* [1986] is used to calculate k_e and k_m is set to a constant value of $39 \times 10^{-7} \; m^2 \; s^{-1}$ except under ice and at the deepest points in the lake.

Sensible and latent heat fluxes from the lake are calculated using the BATS parameterizations *Dickinson et al.* [1993]. The bulk aerodynamic formulations for latent heat flux (F_q) and sensible heat flux (F_s) are as follows,

$$F_q = \rho_a C_D V_a (q_s - q_a) \tag{3.29}$$
$$F_s = \rho_a C_p C_D V_a (T_s - T_a) \tag{3.30}$$

where the subscripts s and a refer to surface and air, respectively; ρ_a is the density of air, V_a is the wind speed, C_p, q is specific humidity, and T is temperature. The momentum drag coefficient, C_D, depends on roughness length and the surface bulk Richardson number.

Under ice-free conditions, the lake surface albedo is calculated as a function of solar zenith angle *Henderson-Sellers* [1986]. Longwave radiation emitted from the lake is calculated according to the Stefan-Boltzmann law. The lake model uses the partial ice cover scheme of *Patterson and Hamblin* [1988] to represent the different heat and moisture exchanges between open water and ice surfaces and the atmosphere, and to calculate the surface energy of lake ice and overlying snow. For further details refer to *Hostetler et al.* [1993] and *Small and Sloan* [1999].

3.2.10 Aerosols and Dust (Chemistry Model)

The representation of dust emission processes is a key element in a dust model and depends on the wind conditions, the soil characteristics and the particle size. Following *Laurent et al.* [2008] and *Alfaro and Gomes* [2001], here the dust emission calculation is based on parameterizations of soil aggregate saltation and sandblasting processes. The main steps in this calculation are: The specification of soil aggregate size distribution for each model grid cell, the calculation of a threshold friction velocity leading to erosion and saltation processes, the calculation of the horizontal saltating soil aggregate mass flux, and finally the calculation of the vertical transportable dust particle mass flux generated by the saltating aggregates. In relation to the BATS interface, these parameterizations become effective in the model for cells dominated by desert and semi desert land cover.

Chapter 4

Future Developments

We have lot of exciting plans for future model improvements, some of which are in a already mature stage and under testing, with some published results, whereas others are done only on the paper in a whishlist for next years. Nevertheless we want to share this with users, to have hints and encourage contributions. Some of the development results/ideas are listed below, in a "time to market" order.

4.1   UFW PBL scheme

One of the deficiencies identified in RegCM3 has been the lack of simulation of low level stratus clouds, a problem clearly tied to the excessive vertical transport in the Holtslag PBL scheme (*O' Brien* [2011]). To address this problem Travis OBrien coupled to the RegCM4 the general turbulence closure parameterization of [*Grenier and Bretherton*, 2001; *Bretherton et al.*, 2004], which we refer to as UW-PBL. This is a 1.5 order local, down-gradient diffusion parameterization in which the velocity scale is based on turbulent kinetic energy (TKE). The TKE is in turn calculated prognostically from the balance of buoyant production/destruction, shear production, dissipation vertical transport and horizontal diffusion and advection. The scheme also parameterizes the entrainment process and its enhancement by evaporation of cloudy air into entrained air. One property of the scheme is the use of a mixing length formulation based on a 2010 paper by Grisogono (ref?) which allows a more realistic description of sharp inversions under strongly stable conditions. The UW-PBL has been so far tested within the RegCM4 framework mostly in midlatitude domains, such as the continental US (where it considerably improved the simulation of low level stratus clouds) and Europe.

This scheme is currently in a SVN branch of the code and will be merged into the main development trunk as soon as the accompanying paper will be published, and will be available in the next model release.

4.2   Tiedtke convection scheme

Adrian Tompkins is developing an adaptation of the ECHAM5.4 *Tiedtke* [1989] cumulus convection scheme for the RegCM model. The code from ECHAM has been ported into RegCM, and extensive testing is planned in the second half of 2011. This option should be available for next model release.

4.3   Chemistry

Fabien Solmon is developing the coupling of RegCM model with the CBMZ chemical module with the Sillmann fast solver.

4.4   Coupling

We have resolved to adopt for the RegCM model a standard model coupling engine: the Earth System Modeling Framework (ESMF). Ufuk Utku Turuncoglu is already adapting model data structures to use the ESMF framework.

First target will be to couple the RegCM model to the Regional Oceanic Modeling System (ROMS) oceanic model, and update the Community Land Surface Model (CLM) to version 4.

4.5   2D parallelization

This long standing limitation of the model in the parallel performances will be faced: we plan to drop altogether the Serial model version (does exist anymore a single core processor?), clean up model parallel code and perform a dynamical 2D decomposition of the model domain.

4.6   Parallel I/O

This is another limit of the current model implementation, where all data need to be gathered by the master processor before being written to disk. Again, if running on a decent cluster, all processors usually have access to disk resources, and a form of parallel I/O will allow a big performance boost as well as a reduction of some of the MPI communication data at the expenses of an increase of the requirements for the cluster I/O channel.

4.7   Semi-Lagrangian dynamic core

A semi-Lagrangian advection scheme for the water vapor and advection tracers will allow a different timestep for the transport schemes, which should result in a performance prize.

4.8   Non-Hydrostatic core

We want to implement the non-hydrostatic core to allow physical downscaling of large scale model simulation under the 20 kilometers limit of the hydrostatic model.

Bibliography

Alfaro, S. C., and L. Gomes, Modeling mineral aerosol production by wind erosion: Emission intensities and aerosol size distributions in source areas, *Journal of Geophysical Research*, *106*, d16, 2001.

Anthes, R. A., A cumulus parameterization scheme utilizing a one-dimensional cloud model, *Mon. Wea. Rev.*, *105*, 270–286, 1977.

Beheng, K. D., A parameterization of warm cloud microphysical conversion processes, *Atmos. Res.*, *33*, 193–206, 1994.

Bretherton, C. S., J. McCaa, and H. Grenier, A new parameterization for shallow cumulus convection and its application to marine subtropical cloud-topped boundary layers. part i: Description and 1d results, *Monthly Weather Review*, *132*, 864–882, 2004.

Briegleb, B. P., Delta-eddington approximation for solar radiation in the ncar community climate model, *J. Geophys. Res.*, *97*, 7603–7612, 1992.

Collins, W. D., et al., The Community Climate System Model version 3 (CCSM3), *Journal of Climate*, *19*, 2122–2143, 2006.

Deardoff, J. W., Efficient prediction of ground surface temperature and moisture with inclusion of a layer of vegetation, *J. Geophys. Res.*, *83*, 1889–1903, 1978.

Dickinson, R. E., *Climate Processes and Climate Sensitivity*, chap. Modeling evapotranspiration processes for three-dimensional global climate models, pp. 52–72, American Geophysical Union, 1984.

Dickinson, R. E., P. J. Kennedy, A. Henderson-Sellers, and M. Wilson, Biosphere-atmosphere transfer scheme (bats) for the ncar community climate model, *Tech. Rep. NCARE/TN-275+STR*, National Center for Atmospheric Research, 1986.

Dickinson, R. E., R. M. Errico, F. Giorgi, and G. T. Bates, A regional climate model for the western United States, *Climatic Change*, *15*, 383–422, 1989.

Dickinson, R. E., A. Henderson-Sellers, and P. J. Kennedy, Biosphere-atmosphere transfer scheme (bats) version 1e as coupled to the ncar community climate model, *Tech. rep.*, National Center for Atmospheric Research, 1993.

Emanuel, K. A., A scheme for representing cumulus convection in large-scale models, *J. Atmos. Sci.*, *48*(21), 2313–2335, 1991.

Emanuel, K. A., and M. Zivkovic-Rothman, Development and evaluation of a convection scheme for use in climate models, *J. Atmos. Sci.*, *56*, 1766–1782, 1999.

Fairall, C., E. Bradley, J. Godfrey, G. Wick, J. Edson, and G. Young, Cool-skin and warm layer effects on sea surface temperature, *Journal of Geophysical Research*, *101*, 1295–1308, 1996.

Fritsch, J. M., and C. F. Chappell, Numerical prediction of convectively driven mesoscale pressure systems. part i: Convective parameterization, *J. Atmos. Sci.*, *37*, 1722–1733, 1980.

Giorgi, F., Two-dimensional simulations of possible mesoscale effects of nuclear war fires, *J. Geophys. Res.*, *94*, 1127–1144, 1989.

Giorgi, F., Simulation of regional climate using a limited area model nested in a general circulation model, *J. Climate*, *3*, 941–963, 1990.

Giorgi, F., and G. T. Bates, The climatological skill of a regional model over complex terrain, *Mon. Wea. Rev.*, *117*, 2325–2347, 1989.

Giorgi, F., and M. R. Marinucci, Validation of a regional atmospheric model over europe: Sensitivity of wintertime and summertime simulations to selected physics parameterizations and lower boundary conditions, *Quart. J. Roy. Meteor. Soc.*, *117*, 1171–1206, 1991.

Giorgi, F., and L. O. Mearns, Introduction to special section: Regional climate modeling revisited, *J. Geophys. Res.*, *104*, 6335–6352, 1999.

Giorgi, F., G. T. Bates, and S. J. Nieman, The multi-year surface climatology of a regional atmospheric model over the western united states, *J. Climate*, *6*, 75–95, 1993a.

Giorgi, F., M. R. Marinucci, and G. T. Bates, Development of a second generation regional climate model (regcm2) i: Boundary layer and radiative transfer processes, *Mon. Wea. Rev.*, *121*, 2794–2813, 1993b.

Giorgi, F., M. R. Marinucci, G. T. Bates, and G. DeCanio, Development of a second generation regional climate model (regcm2) ii: Convective processes and assimilation of lateral boundary conditions, *Mon. Wea. Rev.*, *121*, 2814–2832, 1993c.

Giorgi, F., X. Q. Bi, and Y. Qian, Radiative forcing and regional climatic effects of anthropogenic aerosols over East Asia: A regional coupled climate-chemistry/aerosols model study, *J. Geophys. Res.*, *107*, 2002.

Giorgi, F., X. Q. Bi, and Y. Qian, Indirect vs. direct effects of anthropogenic sulfate on the climate of east asia as simulated with a regional coupled climate-chemistry/aerosol model, *Climatic Change*, *58*, 345–376, 2003a.

Giorgi, F., R. Francisco, and J. S. Pal, Effects of a subgrid-scale topography and land use scheme on the simulation of surface climate and hydrology. part 1: Effects of temperature and water vapor disaggregation., *Journal of Hydrometeorology*, *4*, 317–333, 2003b.

Giorgi, F., J. S. Pal, X. Bi, L. Sloan, N. Elguindi, and F. Solmon, Introduction to the tac special issue: The regcnet network., *Theoretical and Applied Climatology*, *86*, 1–4, 2006.

Grell, G., Prognostic evaluation of assumptions used by cumulus parameterizations, *Mon. Wea. Rev.*, *121*, 764–787, 1993.

Grell, G. A., J. Dudhia, and D. R. Stauffer, Description of the fifth generation Penn State/NCAR Mesoscale Model (MM5), *Tech. Rep. TN-398+STR*, NCAR, Boulder, Colorado, pp. 121, 1994.

Grenier, H., and C. S. Bretherton, A moist pbl parameterization for large-scale models and its application to subtropical cloud-topped marine boundary layers, *Monthly Weather Review*, *129*, 357–377, 2001.

Hack, J. J., B. A. Boville, B. P. Briegleb, J. T. Kiehl, P. J. Rasch, and D. L. Williamson, Description of the ncar community climate model (ccm2), *Tech. Rep. NCAR/TN-382+STR*, National Center for Atmospheric Research, 1993.

Henderson-Sellers, B., Calculating the surface energy balance for lake and reservoir modeling: A review, *Rev. Geophys.*, *24*(3), 625–649, 1986.

Holtslag, A. A. M., and B. A. Boville, Local versus nonlocal boundary-layer diffusion in a global climate model, *J. Climate*, *6*, 1993.

Holtslag, A. A. M., E. I. F. de Bruijn, and H.-L. Pan, A high resolution air mass transformation model for short-range weather forecasting, *Mon. Wea. Rev.*, *118*, 1561–1575, 1990.

Hostetler, S. W., G. T. Bates, and F. Giorgi, Interactive nesting of a lake thermal model within a regional climate model for climate change studies, *Geophysical Research*, *98*, 5045–5057, 1993.

Hsie, E. Y., R. A. Anthes, and D. Keyser, Numerical simulation of frontogenisis in a moist atmosphere, *J. Atmos. Sci.*, *41*, 2581–2594, 1984.

Kiehl, J. T., J. J. Hack, G. B. Bonan, B. A. Boville, B. P. Breigleb, D. Williamson, and P. Rasch, Description of the ncar community climate model (ccm3), *Tech. Rep. NCAR/TN-420+STR*, National Center for Atmospheric Research, 1996.

Kueppers, L., et al., Seasonal temperature response to land-use change in the western united states., *Global and Planetary Change*, *60*, 2008.

Laurent, B., B. Marticorena, G. Bergametti, J. Leon, and N. Mahowald, Modeling mineral dust emissions from the sahara desert using new surface properties and soil database, *Journal of Geophysical Research*, *113*, d14218, 2008.

Lawrence, P., and T. Chase, Representing a new MODIS consistent land surface in the Community Land Model (CLM3.0), *J. Geophys. Res.*, *112*, g01023, 2007.

O' Brien, T. e. a., A new turbulence parameterization in regcm allows long-term mesoscale simulation of marine stratocumuls., *Climate Dynamics*, 2011.

Oleson, K. e. a., Technical description of the Community Land Model (CLM), *Tech. Rep. Technical Note NCAR/TN-461+STR*, NCAR, 2004.

Oleson, K. W., et al., Improvements to the Community Land Model and their impact on the hydrological cycle, *Journal of Geophysical Research-Biogeosciences*, *113*(G1), 2008.

Pal, J. S., E. E. Small, and E. A. B. Eltahir, Simulation of regional-scale water and energy budgets: Representation of subgrid cloud and precipitation processes within RegCM, *J. Geophys. Res.-Atmospheres*, *105*(D24), 29,579–29,594, 2000.

Pal, J. S., F. Giorgi, X. Bi, et al., The ICTP RegCM3 and RegCNET: Regional climate modeling for the developing world, *Bull. Amer. Meteor. Soc.*, *88*, 1395–1409, 2007.

Patterson, J. C., and P. F. Hamblin, Thermal simulation of a lake with winter ice cover, *Limn. Oceanography*, *33*, 323–338, 1988.

Slingo, J. M., A gcm parameterization for the shortwave radiative properties of water clouds, *J. Atmos. Sci.*, *46*, 1419–1427, 1989.

Small, E. E., and L. C. Sloan, Simulating the water balance of the aral sea with a coupled regional climate-lake model, *J. Geophys. Res.*, *104*, 6583–6602, 1999.

Solmon, F., M. Mallet, N. Elguindi, F. Giorgi, A. Zakey, , and A. Konare, Dust aerosol impact on regional precipitation over western africa, mechanisms and sensitivity to absorption properties, *Geophysical Research Letters*, *35*, l24705, 2008.

Steiner, A. L., J. S. Pal, S. A. Rauscher, J. L. Bell, N. S. Diffenbaugh, A. Boone, L. C. Sloan, and F. Giorgi, Land surface coupling in regional climate simulations of the West African monsoon, *Climate Dynamics*, *33*(6), 869–892, 2009.

Sundqvist, H., E. Berge, and J. E. Kristjansson, The effects of domain choice on summer precipitation simulation and sensitivity in a regional climate model, *J. Climate*, *11*, 2698–2712, 1989.

Tiedtke, M., A comprehensive mass flux scheme for cumulus parameterization on large scale models, *Mon. Wea. Rev.*, *117*, 1779–1800, 1989.

Zeng, X., A prognostic scheme of sea surface skin temperature for modeling and data assimilation, *Geophysical Research Letters*, *32*, l14605, 2005.

Zeng, X., M. Zhao, and R. E. Dickinson, Intercomparison of bulk aerodynamic algoriths for the computation of sea surface fluxes using toga coare and tao data, *J. Climate*, *11*, 2628–2644, 1998.

BATS Biosphere-Atmosphere Transfer Scheme

BATS1e Biosphere-Atmosphere Transfer Scheme version 1e

CAM Community Atmosphere Model

CAPE convective available potential energy

CCM Community Climate Model

CCM1 Community Climate Model version 1

CCM2 Community Climate Model version 2

CCM3 Community Climate Model version 3

CLM Community Land Surface Model

CLM0 Common Land Model version 0

CLM2 Community Land Model version 2

CLM3 Community Land Model version 3

CMAP CPC Merged Analysis of Precipitation

CRU Climate Research Unit

CPC Climate Prediction Center

ECMWF European Centre for Medium-Range Weather Forecasts

ERA40 ECMWF 40-year Reanalysis

ESMF Earth System Modeling Framework

ESP Earth Systems Physics

FAO Food and Agriculture Organization of the United Nations

fvGCM NASA Data Assimilation Office atmospheric finite-volume general circulation model

GLCC Global Land Cover Characterization

GCM General Circulation Model

HadAM3H Hadley Centre Atmospheric Model version 3H

ICTP Abdus Salam International Centre for Theoretical Physics

IPCC Intergovernmental Panel on Climate Change

IBIS Integrated BIosphere Simulator

LAI leaf area index

LAMs limited area models

LBCs lateral boundary conditions

MC2 Mesoscale Compressible Community model

MIT Massachusetts Institute of Technology

MM4 Mesoscale Model version 4

MM5 Mesoscale Model version 5

MERCURE Modelling European Regional Climate Understanding and Reducing Errors

NNRP NCEP/NCAR Reanalysis Product

NNRP1 NCEP/NCAR Reanalysis Product version 1

NNRP2 NCEP/NCAR Reanalysis Product version 2

NCAR National Center for Atmospheric Research

NCEP National Centers for Environmental Prediction

PBL planetary boundary layer

PC Personal Computer

PIRCS Project to Intercompare Regional Climate Simulations

PFT plant functional type

PSU Pennsylvania State University

PWC Physics of Weather and Climate

RCM Regional Climate Model

RegCM REGional Climate Model

RegCM1 REGional Climate Model version 1

RegCM2 REGional Climate Model version 2

RegCM2.5 REGional Climate Model version 2.5

RegCM3 REGional Climate Model version 3

RegCM4 REGional Climate Model version 4

RegCNET REGional Climate Research NETwork

RMIP Regional Climate Model Intercomparison Project

ROMS Regional Oceanic Modeling System

SIMEX the Simple EXplicit moisture scheme

SST sea surface temperature

SUBEX the SUB-grid EXplicit moisture scheme

USGS United States Geological Survey

JJA June, July, and August

JJAS June, July, August, and September

JFM January, February, and March